Geophys. J. Int. (2006) **165,** 3–16 doi: 10.1111/j.1365-246X.2006.02915.x

Constraints on mantle anelasticity from geodetic observations, and implications for the J_2 anomaly

David Benjamin,[1] John Wahr,[1] Richard D. Ray,[2] Gary D. Egbert[3] and Shailen D. Desai[4]

[1]*Department of Physics and Cooperative Institute for Research in Environmental Sciences, University of Colorado, Boulder, CO* 80309-0390, *USA. E-mail: wahr@colorado.edu*
[2]*Space Geodesy Branch, NASA Goddard Space Flight Center, Greenbelt, MD, USA* 20771
[3]*College of Oceanic & Atmospheric Sciences, Oregon State University, Corvallis, OR, USA*
[4]*Jet Propulsion Laboratory, California Institute of Technology,* 4800 *Oak Grove Drive, Pasadena, CA* 91109, *USA*

Accepted 2006 January 18. Received 2005 July 13; in original form 2005 July 13

SUMMARY

We use geodetic observations of the Earth to constrain anelasticity in the Earth's mantle at periods between 12 hr and 18.6 yr. The observations include satellite laser ranging (SLR) measurements of 12 hr and 18.6 yr tides in the J_2 component of the gravity field; space-based observations of tidal variations in the Earth's rotation rate; and optical and space-based measurements of the Chandler Wobble period and damping. These geophysical signals are mostly sensitive to the lower mantle. The results suggest the dissipative process could consist of a single absorption band that extends across seismic periods out at least as far as ∼20 yr. The results also require values of the anelastic parameter Q that are smaller than those required by seismic observations. We interpret this as evidence that Q in the lower mantle is frequency dependent. The frequency dependence suggested by the geodetic observations is reasonably consistent with laboratory measurements, though those measurements have only been done on rocks at upper mantle conditions. After fitting and removing the 18.6 yr tide from the SLR J_2 results, we find that the 1998–2002 anomaly present in the original J_2 observations is no longer a singular anomaly in the J_2 residuals, but becomes one of a series of maxima in a quasi-decadal oscillation.

Key words: Earth rotation, Earth tides, J_2 anomaly, mantle anelasticity.

1 INTRODUCTION

There is a large body of evidence suggesting that energy is dissipated when the Earth's mantle is deformed. The mechanisms responsible for this dissipation are not well understood, and are almost certain to be different in different frequency regimes and for different stress levels. The dissipation occurs almost entirely in shear energy. Dissipation of bulk energy (associated with changes in volume) appears to be negligible for most applications.

The most detailed evidence of this anelastic behaviour comes from seismic data, ranging from the attenuation of 1 s body waves to the decay of seismic-free oscillations at periods of up to tens of minutes. Seismic dissipation is usually represented in terms of a quality factor, Q, defined so that during the deformation the fraction of energy lost per cycle is $2\pi/Q$. Seismic observations show that Q in the mantle tends to decrease (i.e. the dissipation tends to increase), as the radius increases from the core–mantle boundary up through the low-velocity zone. Q then increases dramatically at the top of the low-velocity zone, at about 80 km depth. This radial dependence is illustrated in Fig. 1, using Q values from the PREM seismic earth model (Dziewonski & Anderson 1981),

The seismic evidence suggests that Q is only weakly dependent on frequency across the seismic frequency band. In fact, the PREM Q estimates, like those from most other global seismic models, were derived under the assumption that Q is independent of frequency. A more general method of parametrizing the frequency dependence across the seismic band is

$$Q(\omega) = Q_0\left(\frac{\omega}{\omega_0}\right)^{\alpha}, \tag{1}$$

where ω is the frequency, Q_0 is the value of Q at some reference seismic frequency ω_0, and the unknown parameter α depends on the details of the physical process causing the dissipation. Note that a value of $\alpha = 0$ represents a frequency-independent Q. The parametrization in eq. (1) is partly just an *ad hoc* way to represent a slowly varying function of frequency. However, it is also the frequency-domain equivalent of Lomnitz' law of creep as generalized by Jeffreys (1976), and so is consistent with laboratory experiments on rocks. Most laboratory measurements of

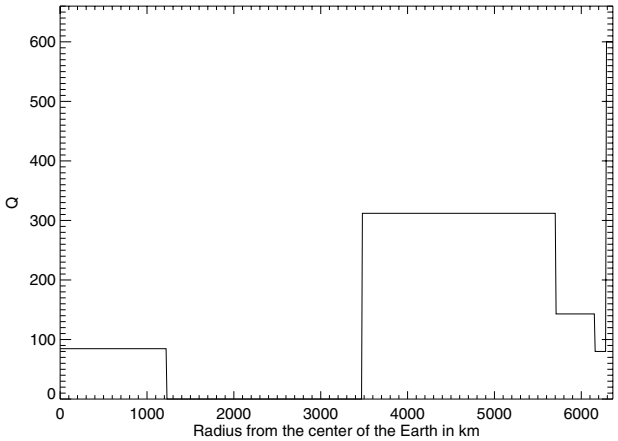

Figure 1. The depth dependence of Q from the seismic model PREM (Dziewonski & Anderson 1981).

Q at seismic and ultraseismic periods, conclude that for rocks at upper mantle pressures and temperatures, α is between 0.15 and 0.40 (see, for example, Gribb & Cooper 1998). This is in direct conflict with the assumption of a frequency-independent Q that is often made when constructing global models such as PREM. There is recent seismic evidence suggesting that Q actually does vary with frequency in the upper mantle. However, even in those studies the results for α, usually between 0 and 0.15 (see, for example, Sobolev *et al.* 1996; Warren & Shearer 2000), tend to be smaller than the laboratory values. Lower mantle results for α are harder to determine, both in the laboratory and for the real earth.

In any real material, Q^{-1} (ω) must vanish at both large and small frequencies, implying that eq. (1) cannot be valid for all values of ω. The extension of the Q model to all frequencies, and the transformation of that model into a shear modulus perturbation, requires discussion.

In the Earth's mantle, dissipation is commonly believed to be caused by an absorption band process (for a summary, see Anderson 1989), meaning that the dissipation occurs at relaxation times spread continuously over some time interval, the 'absorption band' (we will also use the term 'absorption band' to refer to the frequency band corresponding to periods within this time interval). The mathematical distribution of relaxation strengths can be chosen so that for forcing at periods within the absorption band the frequency dependence of Q has the form, eq. (1). In this case both the forcing frequency, ω, and the reference frequency, ω_0, must correspond to periods within the absorption band. In this period range, and for $Q \gg 1$, it can be shown (see, for example, Dahlen & Tromp 1998, eqs 6.111–6.114 combined with 6.23) that the shear modulus, μ, has the form $\mu = \mu_0 + \delta\,\mu$, where

$$\delta\mu(\omega) = \frac{\mu_0}{Q_0}\left[\frac{2}{\pi\alpha}\left\{1 - \left(\frac{\omega_0}{\omega}\right)^{\alpha}\right\} + i\left(\frac{\omega_0}{\omega}\right)^{\alpha}\right] = \frac{\mu_0}{Q_0}[f_r(\omega) + i\,f_i(\omega)], \tag{2}$$

and μ_0 is the real part of the shear modulus at frequency ω_0. The imaginary part of eq. (2) represents dissipation, and the frequency dependence of the real part represents dispersion. Dispersion causes an apparent decrease in μ when the frequency decreases, implying that deformation is larger at longer periods. Dispersion is a necessary by-product of a dissipative mechanism, and is present even when Q is frequency independent, as can be inferred by taking the $\alpha \to 0$ limit of eq. (2):

$$\delta\mu(\omega) = \mu_0\left[\frac{2}{\pi} ln\left(\frac{\omega}{\omega_0}\right) + i\right]\frac{1}{Q_0}. \tag{3}$$

The stress–strain relation for an isotropic solid requires the specification of a second rheological constant (besides μ), which we choose to be the Lamé parameter λ. The effects of anelasticity on λ are determined by the requirement that the bulk dissipation is zero. In that case the bulk modulus, $\kappa = \lambda + \frac{2}{3}\mu$, is real and frequency independent. Thus $\delta\lambda = -\frac{2}{3}\,\delta\mu$.

At forcing periods outside the absorption band, eqs (1) and (2) are no longer valid. Let τ_m and τ_M be the lower and upper bounds of the absorption band. Suppose the resonance strengths are distributed as shown in (6.111) of Dahlen & Tromp (1998), chosen so that eq. (1) is valid at forcing frequencies within the absorption band. We have computed the resulting integrals (6.66)–(6.67) of *Dahlen and Tromp* numerically, to obtain $\mu(\omega)$ at frequencies both inside and outside the absorption band. A few representative results are displayed in Fig. 2, showing f_r and f_i for several values of τ_M. In each case the band's lower bound, τ_m, is taken as 1 s, and $\alpha = 0.25$.

Note that as the period increases beyond τ_M, f_r becomes independent of frequency and $f_i \to 0$. Since Q is proportional to $1/f_i$, this implies that $Q \to \infty$ at long periods. Note also that for frequencies within the absorption band, both the real and the imaginary parts are approximately independent of where the outer edge of the band, τ_M, is located. Thus, although most seismic observations suggest the seismic frequency band lies entirely within an absorption band, they provide no information on how much further out the absorption band extends. One goal of the work described in this paper is to identify the low-frequency limit of the absorption band, by considering long-period geodetic observations. Fig. 2(b) suggests we do this by seeing whether f_i continues to increase with increasing period over our entire range of periods

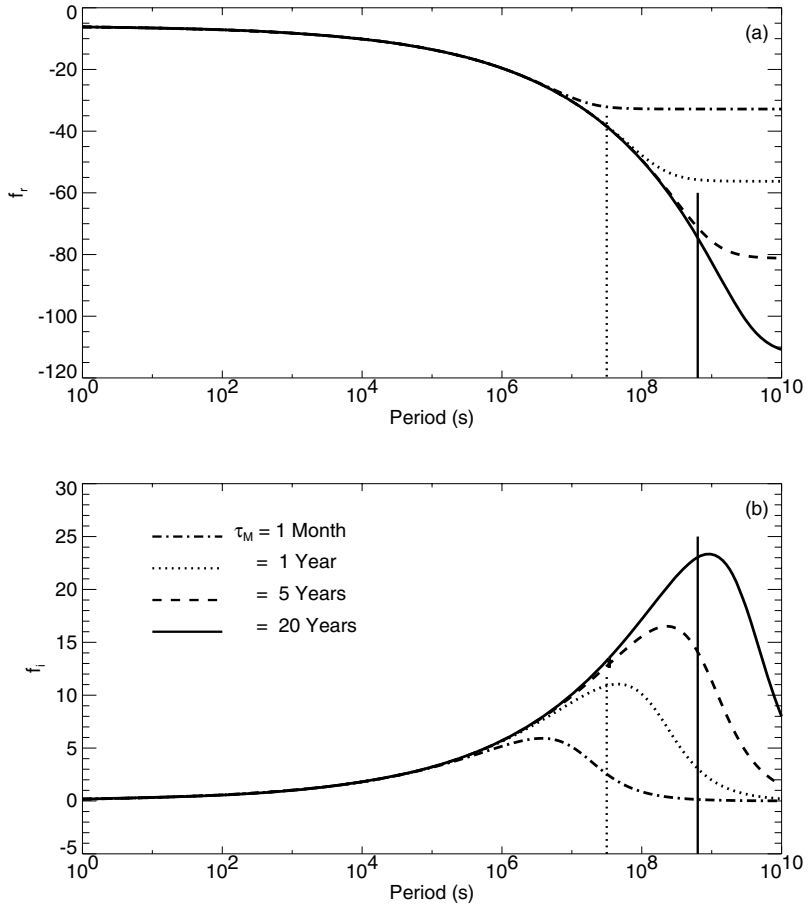

Figure 2. Theoretical results illustrating how the real (a) and imaginary (b) parts of the shear modulus might depend on period for an absorption band model of the dissipative process. The different lines correspond to different models. Each model assumes the same frequency dependence ($\omega^{0.25}$) within the absorption band, and each assumes the same lower limit ($\tau_m = 1$ s) of the absorption band. However, they use different upper limits (τ_M). As examples, the vertical dotted and solid lines indicate the 1 and 20 yr upper limits, used to find the 1 yr and 20 yr solutions. Note, by comparing results for different τ_M's, that the results within an absorption are nearly independent of τ_M. Also, note that the imaginary part, which is proportional to $1/Q$, tends to decrease to zero at periods in excess of τ_M.

(we will find that it does), or whether f_i reaches a maximum at some period and then begins to decrease as the period increases further. A second goal is to use the same geodetic observations to determine whether the frequency dependence of $Q(\omega)$ within the band is consistent with eq. (1) and, if so, to estimate α.

There have been numerous attempts to use geodetic observations to extend anelastic estimates down to subseismic frequencies. These include studies of the period and damping of the 14 month Chandler Wobble (CW) (e.g. Anderson & Minster 1979; Smith & Dahlen 1981), the amplitudes and phase of the 18.6 yr gravity tide and the phase of the M_2 (12 hr) gravity tide (see Eanes 1995; Ray *et al.* 2001, respectively); and the amplitude and phases of the fortnightly (M_f) and monthly (M_m) tidal variations in the Earth's rotation rate (e.g. Dickman & Nam 1998; Defraigne & Smits 1999). In this paper we derive improved results for the tidal variations in rotation rate, construct 18.6 yr tidal estimates based on longer satellite gravity time-series than were available to Eanes (1995), and combine these new results with published results for M_2 and the CW to examine the effects of anelasticity at frequencies between the seismic upper bound of 1 Hz and the 18.6 yr tidal frequency of $\sim 2 \times 10^{-9}$ Hz.

2 INCLUDING ANELASTICITY IN GEOPHYSICAL MODELS

Anelasticity affects these geophysical processes because it plays a role in determining the mantle's deformation in response to applied forces. Mantle deformation is clearly of direct relevance for Earth tides, which are the deformational response of the Earth to the luni–solar tidal force. Its relation to rotation rate arises because deformation generated by the long-period tides changes the Earth's moment of inertia, which requires changes in the rotation rate to conserve angular momentum. In each of these cases (i.e. tidal deformation and tidal variations in rotation rate), the observed signal can be separated into terms that are either in phase or out of phase with the tidal force. The in-phase amplitudes provide constraints on f_r in eq. (2), and the out-of-phase amplitudes constrain f_i.

The CW is a free precession of the Earth's rotation axis relative to the mantle. Its eigenfrequency is partially affected by how the mantle deforms in response to the accompanying variations in centrifugal force. Thus, mantle anelasticity plays a role here too. The CW eigenfrequency is complex, with a real part that is related to the CW period, and an imaginary part related to the damping time. Observations of the period thus constrain f_r, and observations of the damping help determine f_i.

As a specific example of how the geodetic measurements can be used to constrain anelasticity, consider satellite laser ranging (SLR) measurements of the M_2 and 18.6 yr gravity tides. Let $V(r, \theta, \phi)$ be the tidal potential, where r, θ, and ϕ are the radius, colatitude, and eastward longitude, respectively. Let ω represent the frequency of either the M_2 or the 18.6 yr tide. The contribution to V at that frequency has the form (see Cartwright & Tayler 1971):

$$V = Re\left[H_2^m(\omega)\frac{r^2}{a^2}Y_2{}^m(\theta,\phi)e^{i\omega t}\right], \tag{4}$$

where $Y_2{}^m$ is the complex spherical harmonic of degree 2 and order m ($m = 2$ for M_2 and $m = 0$ for the 18.6 yr tide), $H_2^m(\omega)$ represents the amplitude of the tidal force at this frequency, a is the Earth's radius, and Re denotes the real part.

For a spherically symmetric, non-rotating earth, the body tide deformation induced by eq. (4) causes a perturbation, ΔV, in the Earth's external gravitational potential that can be described using the same spherical harmonic:

$$\Delta V = Re\left[k(\omega)\, H_2^m(\omega)\frac{a^3}{r^3}Y_2{}^m(\theta,\phi)e^{i\omega t}\right]. \tag{5}$$

Here, $k(\omega)$ is the gravitational Love number at the frequency ω, and is complex for an anelastic earth. SLR observations can be used to recover tidal amplitudes and phases for this single $Y_2{}^m$ term, and so can be used to constrain $k(\omega)$.

We must model the effects of anelasticity on k. For an anelastic earth, k is complex: the anelastic contribution to the real part of k depends on f_r in eq. (2), and the contribution to the imaginary part depends on f_i. The fact that f_r is dispersive causes the real part of k to be frequency dependent, which leads to frequency dependence for the in-phase component of ΔV. If $\alpha \neq 0$, then the imaginary part of k depends on frequency as well, through the frequency dependence of Q.

We assume $\delta\mu$ is small, and use a first-order expansion to estimate the anelastic perturbation of the Love number k (Smith & Dahlen 1981; Wahr & Bergen 1986):

$$\delta k(\omega) = \int_{\text{mantle}} \left(\frac{\partial k(\omega)}{\partial \mu(r)}\right)_\kappa \delta\mu(r)\, dr, \tag{6}$$

with $\delta\mu$ given by eq. (2). The partial derivative in the integrand in eq. (6) is evaluated using $\mu(r) = \mu_0(r)$ in the equations of motion. Since we are assuming no bulk dissipation, we keep the bulk modulus constant when we take the partial derivative (indicated by the subscript κ after the partial derivative). In most theoretical formulations, including ours, the Lamé parameter λ is used instead of the bulk modulus. In that case the integrand is replaced with:

$$\left(\frac{\partial k(\omega)}{\partial \mu(r)}\right)_\kappa = \left(\frac{\partial k(\omega)}{\partial \mu(r)}\right)_\lambda - \frac{2}{3}\left(\frac{\partial k(\omega)}{\partial \lambda(r)}\right)_\mu, \tag{7}$$

where the subscripts λ and μ indicate that those constants are fixed when finding the derivatives.

Our goal is to learn about $\delta\mu$. The problem is severely underconstrained, even given our assumption of a spherically symmetric earth. There are only a few observations, but there are many possible ways for $\delta\mu$ to vary with frequency and radius. Here we restrict ourselves to a simple parametrization. We assume there is a single absorption band extending from seismic periods up to periods longer than 18.6 yr. We assume μ is given by eq. (3) within the seismic frequency band, to be consistent with the evidence that $Q(\omega)$ is constant across seismic frequencies. However, we allow $Q(\omega)$ to have the more general form (eq. 2) at frequencies below the seismic band. We use ω_m to denote the frequency above which $Q(\omega)$ is independent of frequency, and below which $Q(\omega)$ has the ω^α frequency dependence. Specifically, we assume

$$\begin{aligned}\delta\mu(\omega) &= \frac{\mu_0}{Q_0}\left[f_r(\omega) + i\, f_i(\omega)\right] \\ &= \frac{\mu_0}{Q_0}\begin{bmatrix} \frac{2}{\pi} ln\,(\omega/\omega_0) + i & for\ \omega \geq \omega_m \\ \frac{2}{\pi}\left[ln\,(\omega_m/\omega_0) + \frac{1}{\alpha}\left\{1 - (\omega_m/\omega)^\alpha\right\}\right] + i\,(\omega_m/\omega)^\alpha & for\ \omega < \omega_m \end{bmatrix}.\end{aligned} \tag{8}$$

Moreover, we assume ω_0, ω_m, and α in eq. (8) are radially independent, though we do allow μ_0 and Q_0 to depend on radius. The assumption that ω_0, ω_m, and α are independent of r, is equivalent to assuming that the same physical mechanisms are operative at all depths within the mantle. This is an oversimplification, and it probably tends to bias our recovered values of α toward values appropriate to regions where Q is small (i.e. where the attenuation is large).

To use eq. (8), we must specify ω_0, ω_m, and the functions $Q_0(r)$ and $\mu_0(r)$. The choice of ω_0 has no impact, as long as it is within the frequency-independent seismic band. Here we assume $\omega_0 = 1$ Hz. We consider two values of ω_m. Global seismic models, such as PREM, are usually constructed under the assumption that $Q(r)$ is frequency independent across the entire seismic band, from above 1 Hz (the frequency of body waves) to 3.09×10^{-4} Hz (the frequency of ${}_oS_2$, the longest-period free oscillation). Thus, for our first (and preferred) value we adopt $\omega_m = 3.09 \times 10^{-4}$ Hz. We use the PREM values of $Q(r)$ for $Q_0(r)$, and the 1-Hz PREM values of $\mu\ (r)$ for $\mu_0(r)$. To find the derivative in eq. (7), we also need to specify $\lambda_0(r)$. For this we use $\lambda_0(r) = \kappa_0(r) - \frac{2}{3}\mu_0(r)$, and assume no bulk dissipation so that $\kappa_0(r)$ is the same at all frequencies. We assume $\kappa_0(r)$ is given by its PREM values.

For our second value of ω_m we use $\omega_m = 5.0 \times 10^{-3}$ Hz, corresponding to a period of 200 s. This is the value adopted for the 2003 IERS standards (McCarthy & Petit 2004). We use the same values of $Q_0(r)$, $\mu_0(r)$, and $\lambda_0(r)$ described in the preceding paragraph.

The assumption that ω_0, ω_m, and α are independent of r, is equivalent to assuming that f_r and f_i are independent of radius. In this case, using eq. (8) in eq. (6) leads to:

$$\delta k(\omega) = (f_r + i f_i) \int_{\text{mantle}} \left(\frac{\partial k(\omega)}{\partial \mu(r)} \right)_\kappa \frac{\mu_0(r)}{Q_0(r)}\, dr. \tag{9}$$

Or, equivalently:

$$f_r + i f_i = \frac{\delta k_{\text{obs}}(\omega)}{\int_{\text{mantle}} \left(\frac{\partial k}{\partial \mu} \right)_\kappa \frac{\mu_0}{Q_0}\, dr}, \tag{10}$$

where δk_{obs} is the anelastic perturbation in the Love number k. We evaluate the integral in eq. (10) using the numerical methods described in Wahr & Bergen (1986). δk_{obs} is obtained by using observations to estimate the tidal perturbation in the Earth's gravitational potential ΔV, using eq. (5) to infer k, subtracting the effects of the ocean, and removing the predicted value of k for an elastic earth. The observed tides thus provide information about f_r and f_i at the tidal frequencies. Results are similar for the other observations: for example, the rotation rate variations and the CW period and damping, allowing us to estimate $f_r + if_i$ at a number of subseismic frequencies.

3 EFFECTS OF THE OCEAN

The interpretation of the observations is complicated by the presence of the ocean. For example, the tidal force not only causes the solid earth body tide, but also acts on the ocean to cause ocean tides. The ocean tides load the underlying solid earth and deform it, causing load tides. The ocean + load tides contribute to the observed tidal variations in gravity and rotation rate, and their effects cannot be separated from body tide effects without independent information. These oceanic contributions are small compared to those from the body tide, but they can be of the same order as the anelastic body tide effects. Similarly, the presence of the ocean can significantly modify the CW period and damping. Thus the effects of the ocean must be modelled and removed from the geodetic observations before they can be used to constrain anelasticity. And we must include the effects of ocean model errors when we compute uncertainties in our anelastic estimates.

3.1 An example

An SLR solution for the ${Y_2}^m$ component of ΔV also includes contributions from the ocean + load tide. The spatial dependence of that tide is more complicated than that shown in eq. (5), involving spherical harmonics of all degrees and orders. However, the ocean + load tidal contributions to spherical harmonics other than ${Y_2}^m$ are irrelevant when solving for $k(\omega)$. And because the ${Y_2}^m$ component has a global spatial scale (wavelength ~20 000 km), it is one of the easier ocean + load tidal components to accurately model.

The ocean + load tidal contribution to the ${Y_2}^m$ component of the gravitational potential has the form

$$\Delta V_{\text{load}} = Re\left[\{1 + k'(\omega)\}\, \hat{H}_2^m(\omega) \frac{a^3}{r^3} {Y_2}^m(\theta, \phi) e^{i\omega t} \right], \tag{11}$$

where $\hat{H}_2^m$ is the ${Y_2}^m$ component of the gravitational potential caused by the ocean tide, k' is the load Love number, and the factor "1" in $(1 + k')$ represents the direct gravitational potential of the ocean tide itself. Like k, k' is affected by anelasticity. SLR is sensitive to the sum of eqs (5) and (11). The SLR observations thus provide a constraint on the linear combination $k + (1 + k\prime)\hat{H}_2^m / H_2^m$, which can be used to place bounds on anelasticity if $\hat{H}_2^m$ is adequately known. $\hat{H}_2^m$ is typically on the order of a few percent of H_2^m. Thus, the linear combination is dominated by k, so that it is the body tide that provides most of the anelastic information.

However, knowledge of the ocean tide is still critical. For example, for the 18.6 yr tide $\hat{H}_2^m / H_2^m \approx 0.06$, k and $1 + k'$ are on the order of 0.3 and 0.7 respectively, and anelasticity affects both k and k' at about the 5–10 per cent level. Thus anelastic contributions to $(1 + k\prime)\hat{H}_2^m / H_2^m$ are only about 6 per cent of the anelastic contributions to k, and so can be ignored. However, taken in its entirety, $(1 + k')\hat{H}_2^m / H_2^m$ is roughly twice as large as the anelastic effects on k. So to obtain an estimate of anelasticity accurate to, say, 10 per cent, the Y_2^0 component of the ocean tide must be known to an accuracy of at least 5 per cent. The conclusions are similar for the other observations considered here.

3.2 Ocean models

The anelastic estimates described in this paper require ocean tide models for the M_2, M_f, M_m and 18.6 yr tides, and for the CW pole tide (the response of the ocean to changes in centrifugal force caused by motion of the rotation axis). There are two general methods of estimating ocean tides: using altimeter sea surface height measurements, and finding solutions to the differential equations that describe tidal dynamics. Each method has its characteristic strengths and weaknesses, and many of the most accurate models use a combination of both. Here, we describe the models used for each of the geodetic observations considered in this paper.

The M_2 ocean tide models and their impact on the M_2 anelastic constraint are described by Ray *et al.* (2001). They estimated $\hat{H}_2^2$ by averaging results from four M_2 models that combined Topex/Poseidon (T/P) satellite altimetry and hydrodynamical modelling. One of these

Table 1. Observed values and modelled ocean and elastic earth contributions. The M_2 observed value is from Ray *et al.* (2001), and has had the ocean tide removed. All other observed values include all solid earth and ocean tide contributions. The Chandler Wobble results are from Vicente and Wilson 1997 [V & W], Furuya & Chao (1996) [F & C], and Kuehne *et al.* (1996) [K]. The 18.6 yr results are from the SLR J_2 values, where: [A] the atmosphere has been removed; [B] the atmosphere and ocean circulation have been removed; [C] the atmosphere, ocean circulation, and continental water + snow + ice have been removed.

		Observed	Ocean	Elastic earth
M_2	k_i	-0.0011 ± 0.0003		0
M_f	UT_s (μs)	-779 ± 2	-101 ± 5	-656 ± 7
	UT_c (μs)	48 ± 2	44 ± 5	0
M_m	UT_s (μs)	-838 ± 7	-122 ± 5	-699 ± 7
	UT_c (μs)	29 ± 7	27 ± 5	0
Chandler	Wobble			
V & W	ω_r^{CW} (c yr^{-1})	0.843 ± 0.003	-0.063 ± 0.003	0.927 ± 0.003
	ω_i^{CW} (c yr^{-1})	0.0024 { $0.0005 \leftrightarrow 0.0057$ }	-0.001 ± 0.003	0
F & C	ω_r^{CW} (c yr^{-1})	0.842 ± 0.004	-0.063 ± 0.003	0.927 ± 0.003
	ω_i^{CW} (c yr^{-1})	0.0086 { $0.0042 \leftrightarrow 0.0120$ }	-0.001 ± 0.003	0
K	ω_r^{CW} (c yr^{-1})	0.831 ± 0.004	-0.063 ± 0.003	0.927 ± 0.003
18.6 yr	tide			
A	k_r	0.380 ± 0.02	0.040 ± 0.002	0.298 ± 0.003
	k_i	-0.028 ± 0.008	0.002 ± 0.002	0
B	k_r	0.376 ± 0.03	0.040 ± 0.002	0.298 ± 0.003
	k_i	-0.024 ± 0.008	0.002 ± 0.002	0
C	k_r	0.383 ± 0.02	0.040 ± 0.002	0.298 ± 0.003
	k_i	-0.013 ± 0.007	0.002 ± 0.002	0

was a generalized inverse model that allowed independent assessment of error bars. For the near-resonant ocean responses characteristic of the M_2 tide, strong constraints from T/P altimeter data are critical for arriving at realistic estimates of $\hat{H}_2^2$; unconstrained hydrodynamic models appear to be too sensitive to errors in bathymetry, dissipation, and other factors (Egbert *et al.* 2004).

In contrast, some unconstrained hydrodynamic models of the long-period tides M_f and M_m appear adequate for estimating oceanic perturbations to rotation rate. Estimating the rotation rate is complicated by the need to model the ocean's contributions not only to the Y_2^0 component of sea surface height, but also to the relative angular momentum carried by tidal currents, so hydrodynamic models are required in any event. For this study we use the data assimilating tidal modelling system described in Egbert & Erofeeva (2002) to compute solutions to the shallow water equations forced by the long-period tidal potential, adjusted for effects of body tides, ocean loading, and self-attraction. For M_f a large suite of model runs were completed for a 1/4-degree global grid, and solutions were compared. These runs include time stepping the non-linear equations with quadratic bottom friction and all major tidal constituents, and linearized frequency-domain solutions computed for a range of linear friction parameters. In addition to the forward-model runs, data assimilation experiments were also conducted, fitting T/P altimeter data to varying degrees, using also a range of prior model error covariance assumptions. For almost all cases tested, the computed M_f and M_m effects on rotation rate form tight, consistent clusters, each with a total scatter of about 5 μs in Universal Time. We find similar consistency among these solutions for their effects on polar motion. For polar motion the ocean tide is the primary contributor (Gross *et al.* 1997), and geodetic observations thus provide a direct oceanic constraint, a subject that merits further discussion elsewhere. For now we take these results as evidence that the numerical models for long-period tides are reasonably reliable at the large scales relevant to variations in Earth-rotation parameters, and we use the results from the prior forward model (with no data assimilation) as the ocean corrections given in Table 1. We adopt the 5-μs scatter observed among these models and inversions as an appropriate estimate of the error in these ocean corrections.

Direct ocean measurements are somewhat less useful for the CW pole tide and the 18.6 yr tide. The 18.6 yr tide is virtually impossible to determine using T/P data, given that the altimeter has been in orbit for substantially less than a full tidal cycle, coupled with the fact that the ocean circulation displays strong variability at decadal timescales. The pole tide is somewhat more accessible. Desai (2002), for example, used T/P data to determine the Y_2^1 component of the ocean pole tide, and concluded that at this long wavelength the ocean pole tide is within 3 per cent of equilibrium. At short wavelengths the T/P ocean pole tide solution is subject to the same general problems as the 18.6 yr solution: a relatively short time period and contamination from ocean circulation.

We here make the assumption that the 18.6 yr and pole tides are in equilibrium with the tidal potential. This is equivalent to assuming the barotropic response time of the ocean is much shorter than 18.6 yr and 14 months, respectively. It implies that tidal currents, and the Coriolis and inertial forces induced by those currents, are negligible. An equilibrium tidal response for periods this long is supported by dynamical arguments and by the fact that T/P observations show M_f is close to equilibrium and M_m is closer still (see, for example, Carton 1983; Desai & Wahr 1999; Egbert & Ray 2003), as well as by Desai's (2002) pole tide results.

We use the self-consistent equilibrium ocean pole tide model from Desai (2002), and a similarly derived long-period self-consistent equilibrium model for the 18.6 yr ocean tide. In both cases we modify Desai's model to include effects of mantle anelasticity, as follows. The

equilibrium tides are proportional to $1 + k - h$, where the body tide Love numbers, k and h, are affected by anelasticity. We estimate those anelastic effects, which were not included in Desai's model, using the frequency-dependent anelastic results discussed below (Section 5). We then rescale Desai's model to accommodate our new value of $1 + k - h$. These anelastic effects are small, perturbing the ocean tide by no more than 5 per cent; though they do introduce small out-of-phase components.

4 GEODETIC OBSERVATIONS

In this paper we find constraints on f_r and f_i using observations of the M_2 and 18.6 yr Love number k, the M_f and M_m tidal variations in rotation rate, and the CW period and damping. All numerical results are shown in Tables 1 and 2. Here, we describe the derivation of those results.

For M_2 we use the results of Ray *et al.* (2001), who determined the lag in the Earth's body tide by combining SLR and altimeter tidal estimates; SLR is sensitive to the Love number k, altimetry is most sensitive to h. They modelled the ocean contributions as described in the preceding section. Let the phase lag of the body tide Love number k be expressed as arctan $(-k_i/k_r)$, where k_i and k_r are the imaginary and real parts of k. Ray *et al.* concluded that after removing the effects of the ocean, the phase lag of the M_2 body-tide Love number is $0.204^\circ \pm 0.047^\circ$. Their error analysis accounted for relatively weak constraints on the lags of the load Love numbers k' and h'. They did not attempt to place constraints on the Love number amplitude. However, their results imply that the real and imaginary parts are related by: $k_i = -k_r \times \arctan(0.20^\circ \pm 0.05^\circ) \approx k_r \times (-0.0035 \pm 0.0009)$. We estimate k_r by solving the tidal equations of motion using the 1 s PREM elastic values of μ and λ. We obtain $k_r = 0.298$, implying that $k_i = -0.00105 \pm 0.00027$. Since $k_i = 0$ for an elastic earth, we use this value of k_i for the imaginary part of $\delta k_{\rm obs}$ in eq. (10). Using the numerical methods described by Wahr & Bergen (1986), we find the integral in the denominator of eq. (10) $= -6.18 \times 10^{-4}$. Thus, we estimate $f_i = 1.70$ for the M_2 tide. The value of f_r is unknown in this case, since we have no observational results for the real part of k_r.

For the CW we require observational estimates of the period, T_{CW}, and damping parameter, Q_{CW}. These are combined to form the complex frequency

$$\omega^{CW} = \frac{1}{T_{CW}}\left[1 + i/2Q_{CW}\right]. \tag{12}$$

After correcting for the effects of the ocean, and removing the predictions for an elastic earth, the residual value $\delta\omega^{CW}$ is used to replace $\delta k_{\rm obs}$ in eq. (10). And ω^{CW} is used instead of k in the partial derivative in the denominator.

For T_{CW} and Q_{CW} we use three sets of observational results: Furuya & Chao (1996), Kuehne *et al.* (1996), and a combination of Vicente & Wilson (1997) and Wilson & Vicente (1990). Furuya & Chao (1996) combined 11 yr of space-based observations with an atmospheric excitation time-series, to estimate $T_{CW} = 433.7$ mean solar days and $Q_{CW} = 49$. Kuehne *et al.* (1996) used a similar analysis to obtain $T_{CW} = 439.5$ d, but did not determine Q_{CW}. Vicente and Wilson applied a maximum likelihood technique to astrometric and space-based observations from the mid-19th century to the 1990s, to obtain $T_{CW} = 433.1$ d. They did not solve for Q_{CW}. Instead, based on Vicente and Wilson's suggestion, we combine Vicente and Wilson's T_{CW} estimate with an estimate of $Q_{CW} = 179$ based on a similar analysis by Wilson & Vicente (1990).

To correct for the ocean, we adopt the self-consistent equilibrium tide model described in Section 3.2. To account for the possibility of errors, caused either by non-equilibrium effects or by errors in the ocean function, Love numbers, or ocean density, we assume an uncertainty of ± 5 per cent of the ocean tide estimate and include that uncertainty in both the real and imaginary parts of ω^{CW}. A 5 per cent uncertainty is chosen because of Desai's (2002) results, which imply the long-wavelength components of the pole tide are within 3 per cent of equilibrium. To estimate and remove ω^{CW} for an elastic earth, we use the 1 s numerical values from PREM, and adjust the resulting estimate of ω^{CW} to be consistent with the observed value of the Earth's precession constant as described by Smith & Dahlen (1981). We arbitrarily assume an uncertainty of 0.003 c yr^{-1} in the elastic earth prediction; a value equal to 1 per cent of the deformational contribution to ω^{CW}. To obtain our final uncertainties in f_r and f_i, we add, in quadrature, the uncertainties for the observations, the ocean corrections, and the elastic earth predictions.

We represent the M_f and M_m tidal perturbations in rotation rate in terms of in-phase and out-of-phase contributions to Universal Time, denoted as UT_s and UT_c, respectively. (By convention, the s and c subscripts refer to sine and cosine of the tidal argument; see Gross 1993.) We combine these terms into the complex quantity

$$UT = UT_s + iUT_c, \tag{13}$$

which is used to replace $\delta k_{\rm obs}$ in eq. (10), after subtracting the effects of the ocean and an elastic earth.

The M_f and M_m tidal perturbations in rotation rate are estimated from the SPACE2003 time-series of Earth rotation parameters, produced by Gross (2004) by combining various kinds of space-geodetic measurements. We only use data from 1985 to 2003; earlier data are significantly noisier and also appear somewhat oversmoothed in the tidal bands of interest here. The SPACE2003 rotation-rate data were subsequently adjusted to remove the effects of both the atmosphere and the oceans. Atmospheric angular momentum was determined from the NCEP Reanalysis solutions (Kalnay *et al.* 1996), which are readily available in the form of excitation functions from the IERS Special Bureau for Atmospheres (Salstein *et al.* 1993). Oceanic angular momentum was determined from the ECCO ocean circulation model (Stammer *et al.* 2002), for which the excitation functions were computed by Gross *et al.* (2004). Both the AAM and OAM models result in reduced variance

in the SPACE2003 length-of-day data, a matter discussed in some detail by Gross *et al.* (2004). To further reduce the variance of the original time-series, a low-degree polynomial was fit and removed from the data and a high-pass filter was applied (see, for example, Chao *et al.* 1995).

The estimated tidal rotation parameters are given in Table 1 in terms of UT perturbations. The standard errors are estimated from the least-squares covariance, scaled by the spectral density of the time-series residuals surrounding the monthly and fortnightly frequencies. The residuals at the monthly frequency are significantly larger, which accounts for the relatively larger uncertainty in the M_m estimates. The standard errors for M_f have been checked in two ways—by computing estimates at nearby non-tidal frequencies and by partitioning the time-series and studying the scatter in the subset estimates—and the results of both tests are consistent with the quoted M_f error bars of Table 1.

The M_f and M_m ocean tide contributions are described in Section 3.2. The predictions for an elastic earth are computed using the 1 *s* PREM parameter values, and an additional uncertainty equal to 1 per cent of the elastic predictions is included in the error estimate. The final error is the sum, in quadrature, of the observational, ocean tide and elastic earth errors.

4.1 18.6 yr results and the J_2 anomaly

Our SLR solution for the 18.6 yr Love number requires an expanded discussion. Partly this is because the 18.6 yr tide has the longest period of any process we consider in this paper, and thus it exerts the most leverage on our conclusions. And partly it is because the residuals from the fitting process have implications for interpreting the non-tidal signal in the SLR data.

The coefficient of the Y_2^0 gravity field component is denoted as J_2. Since the 18.6 yr solid earth tide perturbs this component, its effects appear in J_2. We estimate the 18.6 yr Love number k by fitting to two sets of ≈monthly J_2 values derived from SLR data. One set was provided by Chris Cox (personal communication, 2005), and runs from early 1979 to the fall of 2004 (for a description of an earlier version of this data set, see Cox & Chao 2002). The second set was provided by M.K. Cheng (personal communication, 2004) and runs from early 1979 to the beginning of 2004 (Cheng & Tapley 2004). We refer to these J_2 data sets as CC and CT, respectively.

Before sending us the CC values, Cox had removed atmospheric effects using NCEP pressure values and assuming an inverted barometer (IB) response of the oceans. The atmosphere had not been removed from the CT values. To make the two sets compatible, we also subtract the NCEP + IB atmosphere from CT.

Both Cox and Cheng had removed a nominal 18.6 yr tide model: in-phase and out-of-phase solid earth contributions consistent with the 2003 IERS standards (McCarthy & Petit 2004), plus a self-consistent equilibrium ocean tide. Cox and Cheng used different numerical values for the equilibrium ocean tide; so we modified both sets of results to be consistent with Desai's (2002) equilibrium values (see above). The IERS standards assume an anelastic earth, with the same general framework as described in eq. (8), using $\omega_0 = 1$ Hz, $\omega_m = 5.0 \times 10^{-3}$ Hz, and $\alpha = 0.15$. These anelastic assumptions in the IERS standards are based on earlier comparisons with CW and tidal rotation rate observations, and are independent of any 18.6 yr observations.

Fig. 3 compares the CC and CT results, after simultaneously fitting and removing a constant, a trend and seasonal (i.e. annual and semi-annual) terms, and smoothing the residuals with a 24 month boxcar averaging function. The formal errors provided with the data are used in this and all other fits to the J_2 values. There are clear systematic trends remaining in the residuals shown in Fig. 3, that presumably include some combination of long-period gravity signals from the oceans and the water + snow + ice stored on land, errors in the IERS 18.6 yr tidal model, and SLR processing effects. Processing effects clearly remain in one or the other or both of these two sets of residuals, since they exhibit differences. Both data sets do show a common peak from 1998 to about 2002. This anomaly was noticed by Cox & Chao (2002), and has since been interpreted as being at least partly due to the combined effects of the ocean and mountain glaciers (Dickey *et al.* 2002).

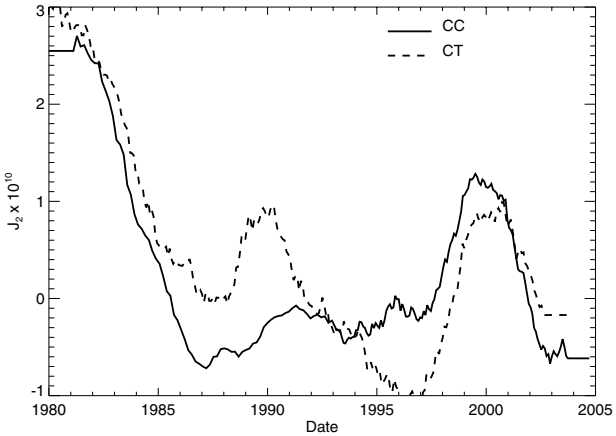

Figure 3. Compares the CC and CT J_2 results. Both data sets have had the effects of the atmosphere + IB ocean removed. An 18.6 yr tide has also been removed, using the solid earth values recommended in the 2003 IERS standards, plus ocean tide values consistent with an equilibrium tide. A linear trend and seasonal terms have been fit and removed from each data set, and the residuals have been smoothed with a 24 month boxcar function.

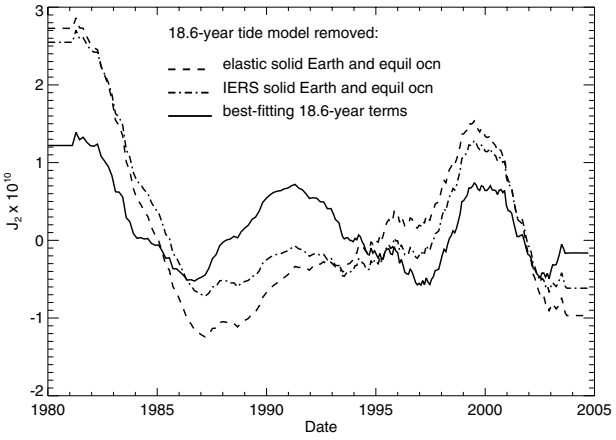

Figure 4. Shows the CC J_2 results, after fitting and removing a linear trend and seasonal terms, and smoothing the residuals. The different lines correspond to removing different models of the 18.6 yr tide before performing this fit.

As noted by Cox *et al.* (2004), this 1998–2002 feature could affect any estimate of the 18.6 yr tide obtained by fitting to the J_2 data. On the other hand, it could also be partly an artefact of a mismodelled 18.6 yr tide. This, in fact, is suggested by Fig. 4, which shows smoothed CC residuals after fitting and removing a trend and seasonal terms, for various assumptions about the 18.6 yr tide. The dashed line shows results after adding back (prior to the fit) the IERS 18.6 yr solid earth model that had been removed during processing, and then removing the 18.6 yr predictions for an elastic earth. So the dashed residuals include the effects of all anelastic contributions to the 18.6 yr tide. Note that those residuals are dominated by a quasi-periodic term that fits about 1.5 cycles into the ≈25 yr data span, which is reasonably consistent with an 18.6 yr variation. The dashed-dotted line shows the results with the IERS corrections removed prior to the fit—or the same CC residuals shown in Fig. 3. Note that although the apparent 18.6 yr term is reduced, it is still reasonably prominent; suggesting that the IERS model does not adequately represent the effects of anelasticity.

The solid line in Fig. 4 shows the residuals after simultaneously fitting and removing in-phase and out-of-phase 18.6 yr terms, along with the trend and seasonal terms. Note that the residuals have changed dramatically so that the 1998–2002 feature is no longer an isolated anomaly, but is just one of a series of maxima in a quasi-decadal oscillation. We have no definitive explanation for this oscillation, but it seems plausible that there could well be a quasi-periodicity of this sort caused by the same types of processes considered by Dickey *et al.* (2002).

Thus we tentatively assume that the 18.6 yr terms we obtain by fitting to the CC and CT values, are true tidal terms. We attempt to improve the fit by simultaneously including a 10 yr term in the fitting process, since the Fig. 4 residuals seem to include such a term. The impact of this additional term on our 18.6 yr solution, however, is minimal.

To test for convergence of our 18.6 yr solutions, we perform these fits for a variety of time intervals, each beginning in 1979 but ending at times that vary between 1996 and the end of the time-series. We do this for both CC and CT, and scale our results so that they directly correspond to perturbations of the Love number k. In each case we add back the IERS 18.6 yr model that had been initially removed from the data. We do not add back the equilibrium ocean tide results. We interpret the final results as the Love number k for the solid, anelastic earth.

Fig. 5 shows our results along with our estimate of the uncertainty in the fitting process. The Fig. 5 uncertainty estimates do not include the uncertainty in the ocean tide or elastic earth models. Results are shown for both the CC and CT models, and for both the real (panel a) and imaginary (panel b) parts of the Love number. Note that the solutions using data up to 2001 and later appear to have converged reasonably well, and to values that depart significantly from the elastic values (the horizontal lines in each panel). The values, though, still appear to be wandering around by an amount larger than the uncertainties in the solutions. Furthermore, although CC and CT give imaginary parts of k that are in reasonable agreement, they give significantly different real parts. This is probably the consequence of the long-period differences between CC and CT apparent in Fig. 3.

To account for all these differences, we choose a range for our final adopted value of k, so that it encompasses the maximum and minimum of all CC and CT fits for endpoints from 2001 onwards. We choose the midpoint of that interval as our preferred value. (We adopt this method of choosing a preferred value because, when combined with symmetric error bars, it provides a convenient way to represent the range of possible values.) We obtain $k_r = 0.339 \pm 0.02$ and $k_i = -0.028 \pm 0.008$, shown as the diamonds in Fig. 5. These numbers represent a 10–15 per cent increase in the Love number over that expected for an elastic earth (see the last column in Table 1).

There is the danger that our fit results could be absorbing the effects of long-period, non-tidal surface mass variability. Our Fig. 5 check for convergence is intended as a partial assessment of that contamination, and our inclusion of a 10 yr periodic term in the final fit is an attempt to reduce that problem. Still, the fact that the SLR data span only ≈1.5 cycles of the 18.6 yr term, requires extra caution.

Thus we repeat our fits, but after first removing an estimate of the J_2 contributions from ocean circulation, as estimated using the ECCO ocean general circulation model (Stammer *et al.* 2002) and provided by S. Marcus and J. Dickey (personal communication, 2005). The 18.6 yr results in this case become $k_r = 0.335 \pm 0.03$ and $k_i = -0.024 \pm 0.008$; so there is no significant impact on k_r, and only a marginally significant impact on k_i. Results obtained by removing alternative ECCO ocean values provided by E. Leuliette (personal

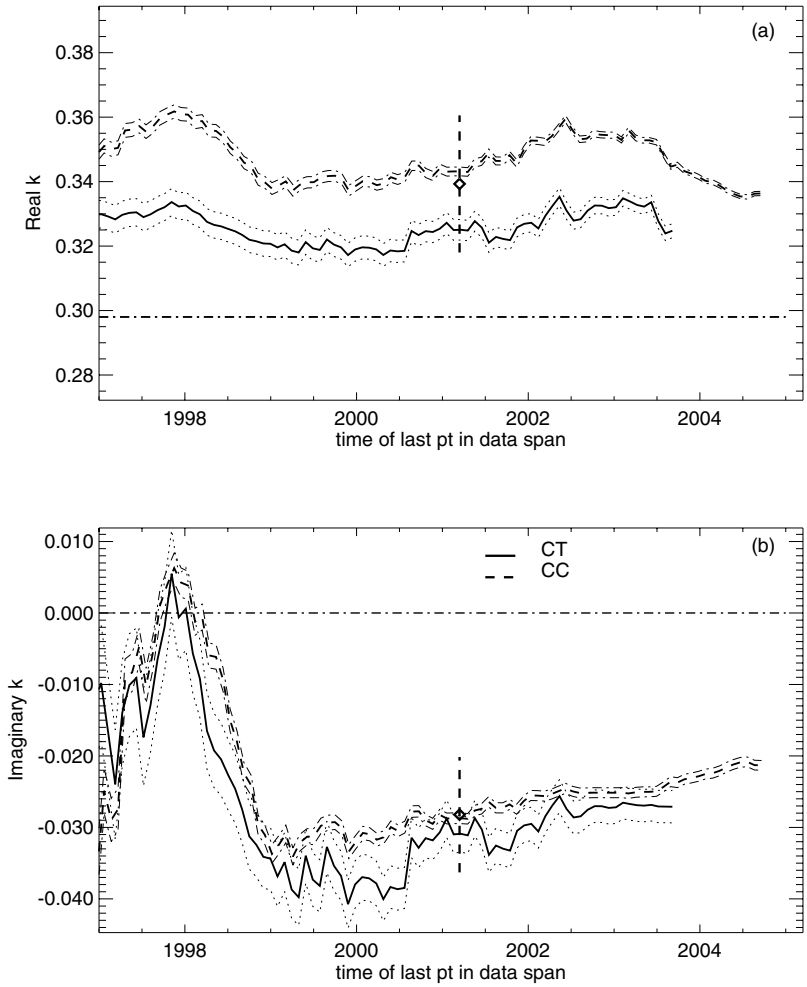

Figure 5. Shows the real (a) and imaginary (b) parts of the 18.6 yr body tide Love number k, obtained by fitting to subsets of CC's and CT's SLR J_2 data set. Each subset uses SLR data between the beginning of 1979 and a variable ending date, as specified on the x-axis. Each set of results is represented by a central line indicating the best-fitting value, bracketed above and below by secondary lines indicating the 1-σ uncertainty from the fitting process. We summarize these results by adopting the overall values and uncertainties denoted by the diamonds and accompanying error bars. The elastic predictions are shown as the horizontal lines.

communication, 2005) are similar. We find that when we compute the variance of the J_2 residuals after fitting and removing a trend and 18.6 yr and seasonal terms, the residual variance is reduced by about 30 per cent in the case where the ocean circulation effects are first removed. This provides confidence in the ocean circulation estimates, and suggests we place more faith in the $k_r = 0.335$ and $k_i = -0.024$ values.

We also repeat the fits, after first removing not only the ECCO ocean circulation estimates, but also estimates of the J_2 contributions from continental glaciers and land water + snow storage as provided by S. Marcus and J. Dickey (personal communication, 2005). The Love number results in this case become, $k_r = 0.340 \pm 0.02$ and $k_i = -0.013 \pm 0.007$, which are about the same as the results from the original data set. We find, though, that the removal of the continental water + snow + ice estimates results in a $\approx$10 per cent increase in the post-fit variance, suggesting that those corrections may not be as reliable as the ECCO ocean corrections.

Table 1 includes the Love number results for all three cases (using the J_2 values as given, removing the ocean circulation effects, and also removing the continental water + snow + ice effects). Table 2 shows the corresponding results for f_r and f_i, and their uncertainties. Those uncertainties are the quadrature sum of the three error types indicated in Table 1: the observational errors, an uncertainty of 5 per cent in the equilibrium ocean tide correction, and a 1 per cent uncertainty in the elastic solid earth correction.

5 IMPLICATIONS FOR ANELASTICITY

The Table 2 results for f_r and f_i are shown as a function of frequency in Fig. 6. Also shown are predictions from eq. (8) for a few values of α, assuming $\omega_0 = 1$ Hz and $\omega_m = 3.09 \times 10^{-4}$ Hz. For an elastic earth, f_r and f_i would both equal 0.

The observations clearly require anelasticity. They also strongly support the hypotheses that Q decreases with increasing period (compare the observations with the constant-Q predictions). It appears as though the results for f_i are still increasing with increasing period out at least

Table 2. Shows the values of f_r and f_i for each observation. The notation denoting the different Chandler Wobble and 18.6 yr tidal results, is the same as in Table 1.

	f_r	f_i
M_2	NA	1.7 ± 0.4
M_f	-16 ± 6	3 ± 4
M_m	-12 ± 9	2 ± 6
Chandler Wobble		
V & W	-24 ± 6	$4\ \{-2 \leftrightarrow 8\}$
F & C	-25 ± 6	$11\ \{5 \leftrightarrow 17\}$
K	-38 ± 6	NA
18.6 yr tide		
A	-69 ± 35	49 ± 14
B	-61 ± 47	42 ± 14
C	-70 ± 39	24 ± 13

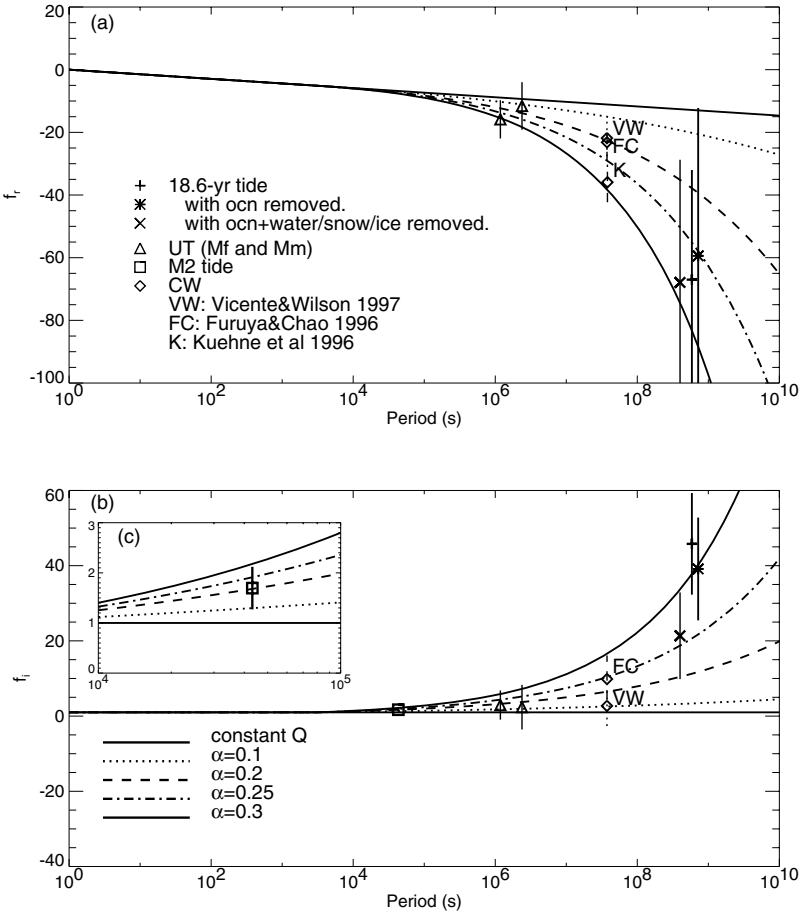

Figure 6. Compares our various observational results for f_r (a) and f_i (b), with predictions from eq. (10) for five anelastic models. Each model assumes $\omega_m = 3.09 \times 10^{-4}$ Hz, but is characterized by a different value of α. Inset (c) is an expanded picture of the M_2 f_i value.

as far as 18.6 yr. This is consistent with a single absorption band that extends from seismic periods out at least as far as ≈20 yr or so (see Fig. 2, and the discussion in Section 1). The results are all reasonably consistent with a single value of α of between about 0.20 and 0.30.

The observations considered in this paper are far more sensitive to the lower mantle (i.e. to depths below 660 km) than to the upper mantle. We find the contribution of the lower mantle to the integral in eq. (9) is about 10 times larger than the contribution from the upper mantle. Thus, if we allowed the upper and lower mantles to have different values for $(f_r + if_i)$, the observations would be about 10 times more sensitive to the lower mantle value than to the upper mantle value. Thus, the results shown in Fig. 6 and the conclusions drawn from those results should be interpreted as mostly representative of the lower mantle.

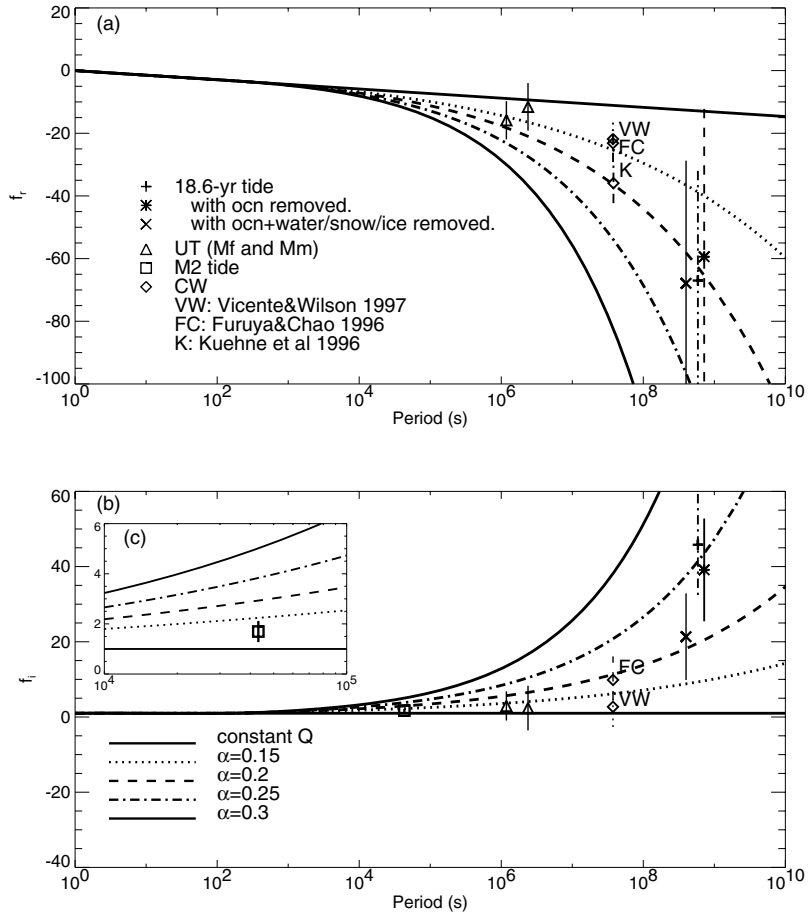

Figure 7. Similar to Fig. 6, but assumes $\omega_m = 5.0 \times 10^{-3}$ Hz.

Our choice of $\omega_m = 3.09 \times 10^{-4}$ Hz is relatively arbitrary. To consider the effects of this choice, we recompute the predictions from eq. (8), using the value $\omega_m = 5.0 \times 10^{-3}$ Hz adopted for the IERS standards (McCarthy & Petit 2004). Fig. 7 compares these new predictions with the observations. The new results do not alter our conclusion that Q decreases with increasing period, or that the observations are consistent with a single absorption band. The observations, in general, appear to require somewhat smaller values of α, somewhere within the range of 0.15 (the value adopted for the IERS standards) and 0.25. Note, though, that for this new choice of ω_m, it becomes harder to reconcile all the observations using a single value of α. The M_2 f_i result, for example, appears to require a significantly smaller value of α than does the 18.6 yr f_i result.

6 DISCUSSION

We have used geodetic observations to constrain mantle anelasticity at periods between 12 hr and 18.6 yr. Our results are ≈10 times more sensitive to the lower mantle than to the upper mantle, and so our constraints should mostly be interpreted as constraints on lower mantle anelasticity.

Our primary goal is to help provide information about whether the physical mechanisms responsible for anelasticity at seismic periods could also be dominant at these longer periods. It should be clear from the outset that we cannot provide a definitive answer to this question, given the small number of observations at our disposal compared to the many ways in which anelasticity could depend on frequency and radius. The issue is further complicated by the fact that anelastic mechanisms could conceivably depend on the stress amplitude, which we are not including in our parametrization. The stresses generated during our geodetic disturbances are far larger than typical seismic stresses. Stress amplitudes are on the order of 6×10^4 Pa for the M_2 tide, 3×10^3 to 6×10^3 Pa for the M_f, M_m, and 18.6 yr tides, and 2×10^2 Pa for the CW. To compare with seismic stresses, note that the stress amplitude associated with the ${}_0S_2$ free oscillation, which has a radial structure that closely resembles that of the tidal and CW deformations, was on the order of only 1 Pa following the magnitude 8.3, 1994 Bolivian earthquake, the largest deep earthquake ever recorded.

The most striking implication of our analysis is that despite the differences in frequency and stress, models that use seismic Q values are in fairly good agreement with all our geodetic observations. It seems reasonable to expect that the seismic anelastic mechanisms would still

be operative at periods somewhat outside the seismic band. What this first implication suggests is that these mechanisms could be operative out at least as far as 18.6 yr, and that they are not likely to depend strongly on the stress amplitude.

A second implication is that within our range of geodetic periods, f_i (proportional to Q^{-1}) increases steadily with increasing period. This has two, somewhat contradictory, implications. The fact that this steady increase appears to continue out to at least 18.6 yr, suggests that not only might seismic mechanisms still be operative at 18.6 yr, but that those mechanisms might be organized into a single absorption band that extends across the seismic band and out to at least ≈20 yr or longer. On the other hand, the fact that the geodetic Q's are frequency dependent at all, appears to put them at odds with the usual seismic assumption that lower mantle Q is frequency independent across the seismic band. This difference, though, is not necessarily incompatible with the assumption of a single seismic–geodetic absorption band, since there are no *a priori* constraints that we know of on how Q should vary with frequency across an absorption band.

A third implication is that across the geodetic band the variation of Q with frequency is reasonably well represented by an ω^{α} dependence. This is a common parametrization of Q that is consistent with laboratory experiments. We find the geodetic observations can be fit reasonably well with a value of α within the range 0.15 to 0.30. This range, though, depends on our choice of ω_m, the frequency below which the constant-Q seismic results begin varying with frequency. For our preferred choice of $\omega_m = 3.09 \times 10^{-4}$ Hz, which is the frequency of the longest-period seismic-free oscillation, the approximate range of α is 0.20 to 0.30. For $\omega_m = 5.0 \times 10^{-3}$ Hz, the value adopted for the IERS standards, the range is reduced slightly to 0.15–0.25; though the use of an ω_m this large makes it difficult to reconcile both the M_2 and 18.6 yr observations with a single value of α. If, instead, we chose ω_m to be smaller than $\omega_m = 3.09 \times 10^{-4}$ Hz, the preferred values of α become larger than 0.20–0.30. If ω_m is chosen to be smaller than about 5×10^{-5} Hz ≈1 cycle 6 hr^{-1}, no value of α could provide an acceptable fit to both the M_2 and 18.6 yr observations.

Interestingly, although our preferred range for α across the geodetic band differs from the usual seismic assumption of $\alpha = 0$ in the lower mantle, it is in reasonable agreement with the laboratory estimates of $\alpha \approx 0.15$–0.40 inferred from experiments on rocks at upper mantle conditions and seismic periods (see, for example, Gribb & Cooper 1998). This agreement may be spurious, since our results are most sensitive to Q in the lower mantle. On the other hand, the fact that our α values are more consistent with those from laboratory experiments than from seismic observations, could conceivably reflect a dependence of Q on stress amplitude. Like geodetic stress levels, laboratory stresses (typically on the order of 10^4 to 10^6 Pa) are much larger than seismic stress amplitudes.

One of the important constraints in this study is provided by our fit of an 18.6 yr tidal term to the monthly SLR J_2 values. As a by-product of our analysis, we find that when we fit and remove an 18.6 yr term from the J_2 values, the 1998–2002 anomaly changes character, becoming only one of a series of maxima in a quasi-decadal oscillation. We have no immediate explanation of the likely cause of this oscillation, though it could well be due to the sorts of environmental processes (oceans, continental water + snow + ice) considered by Dickey *et al.* (2002).

ACKNOWLEDGMENTS

We thank Chris Cox and M.K. Cheng for providing their monthly SLR estimates of the J_2 component of the Earth's gravity field; and S. Marcus, J. Dickey, and E. Leuliette for providing estimates of environmental contributions to J_2. We thank Chris Cox, Richard Eanes, and M.K. Cheng for helpful discussions. This work was partially supported by NASA grants NAG5-7703 and NGT5-50320 to the University of Colorado, and NASA grant NAG5-9159 to Oregon State University. The work performed by SDD was performed at the Jet Propulsion Laboratory, California Institute of Technology under a contract with the National Aeronautics and Space Administration.

REFERENCES

Anderson, D.L., 1989. *Theory of the Earth*, Blackwell Scientific Publications, Boston, p. 366.

Anderson, D.L. & Minster, J.B., 1979. The frequency dependence of Q in the Earth and implications for mantle rheology and Chandler wobble, *Geophys. J. R. astr. Soc.*, **58,** 431–440.

Carton, J.A., 1983. The variation with frequency of the long-period tides, *J. geophys. Res.*, **88,** 7563–7571.

Cartwright, D.E. & Tayler, R.J., 1971. New computations of the tide-generating potential, *Geophys. J. R. astr. Soc.*, **23,** 45–74.

Chao, B.F., Merriam, J.B. & Tamura, Y., 1995. Geophysical analysis of zonal tidal signals in length of day, *Geophys. J. Int.*, **122,** 765–775.

Cheng, M. & Tapley, B.D., 2004. Variations in the Earth's oblateness during the past 28 years, *J. geophys. Res.*, **109,** B09402.

Cox, C.M. & Chao, B.F., 2002. Detection of a large-scale mass redistribution in the terrestrial system since 1998, *Science*, **297,** 831–832.

Cox, C.M., Au, A., Boy, J.-P. & Chao, B.F., 2004. Time-variable gravity: Using satellite-laser-ranging as a tool for observing long-term changes in the Earth system, Proceedings from the 13'th International Workshop on Laser Ranging, eds Noomen, R., Klosko, S., Noll, C. & Pearlman, M., NASA/CP-2003-212248, 2003.

Dahlen, F.A. & J. Tromp, 1998. *Theoretical Global Seismology*, Chapter 6, Princeton University Press, Princeton, NJ.

Defraigne, P. & Smits, I., 1999. Length of day variations due to zonal tides for an inelastic Earth in non-hydrostatic equilibrium, *Geophys. J. Int.*, **139,** 563–572.

Desai, S., 2002. Observing the pole tide with satellite altimetry, *J. geophys. Res.*, **107**(C11), Art. No. 3186.

Desai, S. & Wahr, J., 1999. Monthly and fortnightly tidal variations of the Earth's rotation rate predicted by a TOPEX/POSEIDON empirical ocean tide model, *Geophys. Res. Lett.*, **26,** 1035–1038.

Dickey, J.O., Marcus, S.L., de Viron, O. & Fukumori, I., 2002. Recent Earth oblateness variations: unraveling climate and postglacial rebound effects, *Science*, **298,** 1975–1977.

Dickman, S.R. & Nam, Y.S., 1998. Constraints on Q at long periods from Earth's rotation, *Geophys. Res. Lett.*, **25,** 211–214.

Dziewonski, A. & Anderson, D.L., 1981. Preliminary reference Earth model, *Phys. Earth planet. Inter.*, **25,** 297–356.

Eanes, R.J., 1995. A study of temporal variations in Earth's gravitational field using LAGEOS-1 laser ranging observations, *PhD thesis*, Univ. of Texas at Austin, p. 128.

Egbert, G.D. & Erofeeva, S.Y., 2002. Efficient inverse modeling of barotropic ocean tides, *J. Atmos. Oceanic Tech.*, **19,** 183–204.

Egbert, G.D. & Ray, R.D., 2003. Deviation of long-period tides from equilibrium: kinematics and geostrophy, *J. Phys. Oceanography*, **33,** 822–839.

Egbert, G.D., Ray, R.D. & Bills, B.G., 2004. Numerical modeling of the global semidiurnal tide in the present day and in the Last Glacial Maximum, *J. geophys. Res.*, **109,** C03003.

Furuya, M. & Chao, B.F., 1996. Estimation of period and *Q* of the Chandler Wobble, *Geophys. J. Int.*, **127,** 693–702.

Gribb, T.T. & Cooper, R.F., 1998. Low-frequency shear attenuation in polycrystalline olivine: Grain boundary diffusion and the physical significance of the Andrade model for viscoelastic rheology, *J. geophys. Res.*, **103,** 27 267–27 279.

Gross, R.S., 1993. The effect of ocean tides on the Earth's rotation as predicted by the results of an ocean tide model, *Geophys. Res. Lett.*, **20,** 293–296.

Gross, R.S., 2004. Combinations of Earth orientation measurements: SPACE2003, COMB2003, and POLE 2003, *JPL Publ. 04-12*, Jet Propulsion Lab., Pasadena, p. 20.

Gross, R.S., Chao, B.F. & Desai, S.D., 1997. Effect of long-period ocean tides on the Earth's polar motion, *Progr. Oceanogr.*, **40,** 385–397.

Gross, R.S., Fukumori, I., Menemenlis, D. & Gegout, P., 2004. Atmospheric and oceanic excitation of length-of-day variations during 1988–2000, *J. geophys. Res.*, **109,** B01406.

Jeffreys, H., 1976. *The Earth: Its Origin History and Physical Constitution*, 6th edn, Cambridge University Press, London, 574 pages.

Kalnay, E. et al., 1996. The NCEP/NCAR 40-year reanalysis project. *Bull. Amer. Met. Soc.*, **77,** 437–471.

Kuehne, J., Wilson, C.R. & Johnson, S., 1996. Estimates of the Chandler Wobble frequency and *Q*, *J. geophys. Res.*, **101,** 13 573–13 579.

McCarthy, D.D. & Petit, G., (eds), 2004. IERS Conventions (2003), International Earth Rotation and Reference Service (IERS) Technical Note No. 32.

Ray, R.D., Eanes, R.J. & Lemoine, F.G., 2001. Constraints on energy dissipation in the Earth's body tide from satellite tracking and altimetry, *Geophys. J. Int.*, **144,** 471–480.

Salstein, D.A., Kann, D.M., Miller, A.J. & Rosen, R.D., 1993. The sub-bureau for atmospheric angular-momentum of the International Earth Rotation Service—a meteorological data center with geodetic applications, *Bull. Amer. Met. Soc.*, **74,** 67–80.

Smith, M.L. & Dahlen, F.A., 1981. The period and *Q* of the Chandler Wobble. *Geophys. J. R. astr. Soc.*, **64,** 223–282.

Sobolev, S.B., Zeyen, H., Stoll, G., Werling, F., Altherr, R. & Fuchs, K., 1996. Upper mantle temperatures from teleseismic tomography of French massif Central including effects of composition, mineral reactions, anharmonicity, anelasticity and partial melt, *Earth planet. Sci. Lett.*, **139,** 147–163.

Stammer, D., Wunsch, C., Fukumori, I. & Marshall, J.A., 2002. State estimation in modern oceanographic research, *Eos, Trans. Am. geophys. Un.*, **83**(27), 289, 294–295.

Vicente, R.O. & Wilson, C.R., 1997. On the variability of the Chandler frequency, *J. geophys. Res.*, **102,** 20 439–20 445.

Wahr, J.M. & Bergen, Z., 1986. The effects of mantle anelasticity on nutations, Earth tides, and tidal variations in rotation rate, *Geophys. J. R. astr. Soc.*, **87,** 633–668.

Warren, L.M. & Shearer, P.M., 2000. Investigating the frequency dependence of mantle Q by stacking P and PP spectra, *J. geophys. Res.*, **105**(B11), 25 391–25 402.

Wilson, C.R. & Vicente, R.O., 1990. Maximum likelyhood estimates of polar motion parameters, in *Variations in Earth Rotation*, pp. 151–156, eds McCarthy, D.D. & Carter, W.E., Geophysical Monograph 59.